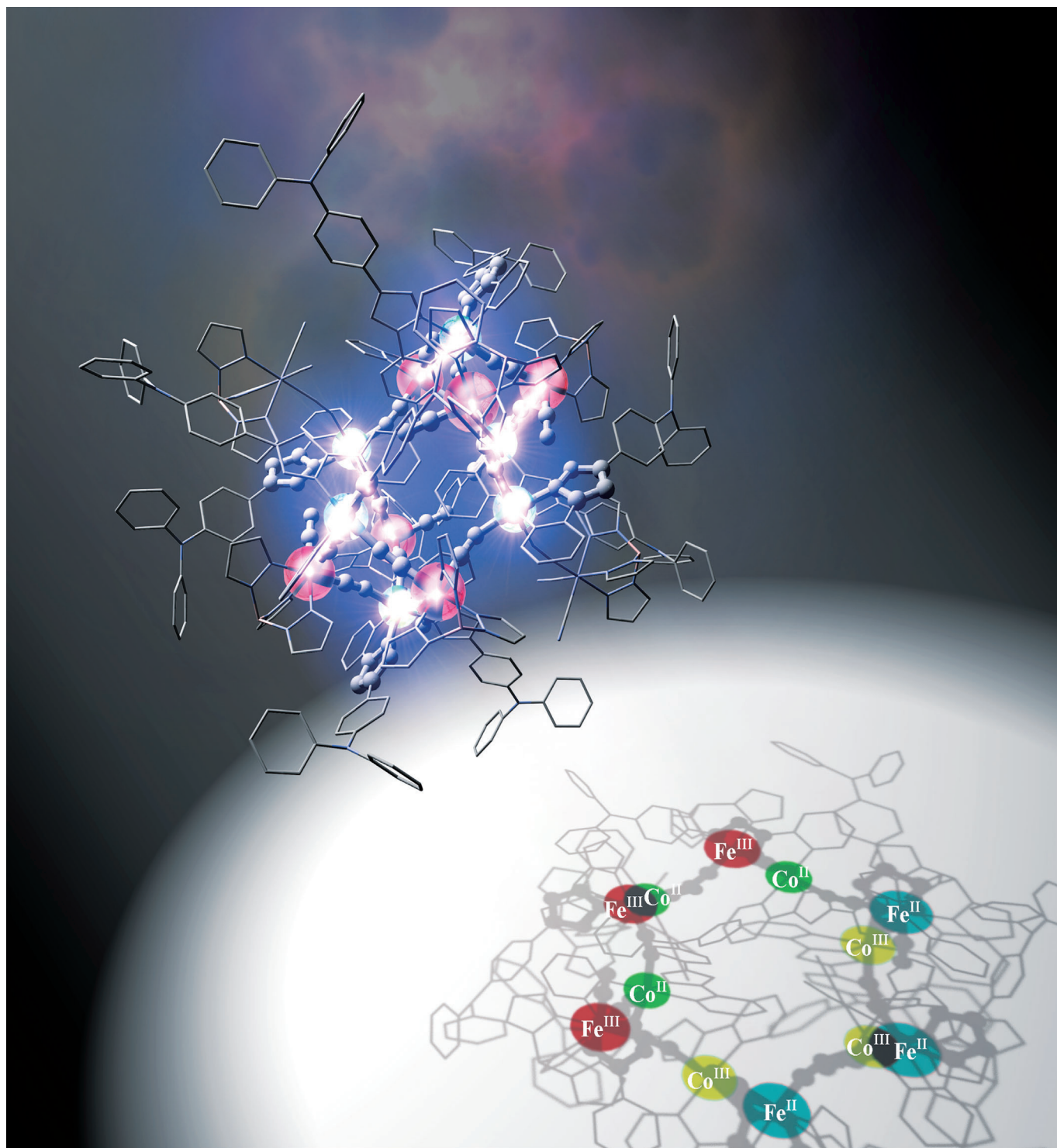


Cyanide-Bridged $[\text{Fe}_8\text{M}_6]$ Clusters Displaying Single-Molecule Magnetism ($\text{M}=\text{Ni}$) and Electron-Transfer-Coupled Spin Transitions ($\text{M}=\text{Co}$)

Kiyotaka Mitsumoto, Emiko Oshiro, Hiroyuki Nishikawa, Takuya Shiga,
Yasuhisa Yamamura, Kazuya Saito, and Hiroki Oshio*^[a]



Abstract: Cyanide-bridged metal complexes of $[\text{Fe}_8\text{M}_6(\mu\text{-CN})_{14}(\text{CN})_{10}(\text{tp})_8(\text{HL})_{10}(\text{CH}_3\text{CN})_2]\text{-}[\text{PF}_6]_4 \cdot n\text{CH}_3\text{CN} \cdot m\text{H}_2\text{O}$ ($\text{HL} = 3\text{-(2-pyridyl)-5-[4-(diphenylamino)phenyl]-1H-pyrazole}$), $\text{tp}^- = \text{hydrotris(pyrazolyl)borate}$), **1**: $\text{M} = \text{Ni}$ with $n = 11$ and $m = 7$, and **2**: $\text{M} = \text{Co}$ with $n = 14$ and $m = 5$) were prepared. Complexes **1** and **2** are isomorphous, and crystallized in the monoclinic space group $P2_1/n$. They have tetradecanuclear cores composed of eight low-spin (LS) Fe^{III} and six

high-spin (HS) M^{II} ions ($\text{M} = \text{Ni}$ and Co), all of which are bridged by cyanide ions, to form a crown-like core structure. Magnetic susceptibility measurements revealed that intramolecular ferro- and antiferromagnetic interactions are operative in **1** and in a fresh

sample of **2**, respectively. AC magnetic susceptibility measurements of **1** showed frequency-dependent in- and out-of-phase signals, characteristic of single-molecule magnetism (SMM), while desolvated samples of **2** showed thermal- and photoinduced intramolecular electron-transfer-coupled spin transition (ETCST) between the $[(\text{LS-Fe}^{\text{II}})_3(\text{LS-Fe}^{\text{III}})_5(\text{HS-Co}^{\text{II}})_3(\text{LS-Co}^{\text{III}})_3]$ and the $[(\text{LS-Fe}^{\text{III}})_8(\text{HS-Co}^{\text{II}})_6]$ states.

Keywords: cluster compounds • cyanide • magnetic properties • single-molecule magnets • transition metals

Introduction

Cyanide ions are useful tools in the assemblies of metal ions into complexes; from zero-dimensional clusters up to three-dimensional arrays. Cyanide bridges propagate magnetic and electronic interactions, and indeed some Prussian blue analogues^[1] have shown magnetic ordering^[1a-c] and multifunctional magnetic properties, such as photomagnetism,^[1d] multiferroics,^[1f] and ionic conductivity in molecular magnets.^[1g] Cyanide-bridged discrete molecules have been synthesized in a wide range of shapes and arrangements such as squares,^[2] cubes,^[3] and trigonal bipyramids.^[4] These have also been afforded considerable attention for their physical properties, such as multistep redox,^[2a,3c] spin crossover,^[2b] single-molecule magnetism (SMM),^[3a,4a] and charge-transfer-induced spin transitions (CTIST).^[2d,3b,4b,c] It should be mentioned that the term “charge transfer” is often used to describe both cases in which a fraction of the charge is shared between two sites or when a complete transfer of charge has occurred with no electron delocalization. The latter case may simply be termed “electron transfer”. Photoinduced CTIST follows a multistep pathway; firstly charge transfer from the $[(\text{LS-Fe}^{\text{II}})(\text{LS-Co}^{\text{III}})]$ to the $[(\text{LS-Fe}^{\text{III}})(\text{LS-Co}^{\text{II}})]$ state, meaning that the valence electron is delocalized both on the iron and cobalt sites. Secondly, the low-spin Co^{II} ion with an $S = 1/2$ undergoes spin transition to reach the HS state of $[(\text{LS-Fe}^{\text{III}})(\text{HS-Co}^{\text{II}})]$, in which the valence electron becomes localized on the Co^{II} ion.^[1b] The thermally induced process is, on the other hand, an entropy-driven phenomenon, and occurs in one step, that is, electron transfer does not “induce” the spin transition. Thus, we use a term which applies equally to the thermal- and light-induced processes

in our systems; electron-transfer-coupled spin transition (ETCST). It should be noted that such discrete ETCST systems are expected to switch between their low- and high-spin states by light irradiation, and such a photoinduced high-spin phase may be an SMM.^[3b] However, metal ions in multinuclear complexes are assembled by bridging ligands, and weak intramolecular interactions such as hydrogen bonds can be used to stabilize unique and unexpected molecular structures.^[5] To take advantage of intramolecular hydrogen bonds in the construction of unique structures, a new ligand ($\text{HL} = 3\text{-(2-pyridyl)-5-[4-(diphenylamino)phenyl]-1H-pyrazole}$) with acidic protons was prepared. The HL ligand has a proton donor site on the pyrazole moiety that can form intramolecular hydrogen bonds, while its bulky triaryl amine substituent is expected to separate molecules by hindering intermolecular hydrogen bonds. Herein we report the syntheses and magnetic properties of two novel heterometal clusters, $[\text{Fe}_8\text{M}_6(\text{CN})_{24}(\text{tp})_8(\text{HL})_{10}(\text{CH}_3\text{CN})_2]\text{-}[\text{PF}_6]_4 \cdot n\text{CH}_3\text{CN} \cdot m\text{H}_2\text{O}$ (**1**: $\text{M} = \text{Ni}$, $n = 11$, $m = 7$ and **2**: $\text{M} = \text{Co}$, $n = 14$, $m = 5$; $\text{tp}^- = \text{hydrotris(pyrazolyl)borate}$)), which exhibit SMM and ETCST behaviors, respectively.

Results and Discussion

Structure descriptions: Complexes **1** and **2** were prepared by the reactions of HL, $\text{M}[\text{BF}_4]_2 \cdot 6\text{H}_2\text{O}$ ($\text{M} = \text{Ni}$ for **1**, and $\text{M} = \text{Co}$ for **2**) with $n\text{Bu}_4\text{N}[\text{Fe}(\text{CN})_3(\text{tp})]^{[2e]}$ and $n\text{Bu}_4\text{NPF}_6$ in CH_3CN . The structure of **2**⁴⁺ at 93 K is shown in Figure 1. Complexes **1** and **2** are isostructural and crystallize in the monoclinic space group of $P2_1/n$. Cations of both complexes are located on the crystallographic inversion center, and charge balance, coordination bond lengths, and Mössbauer data (Figure S1 and S2) suggest that the complex cations are composed of eight low-spin (LS) Fe^{III} and six Ni^{II} (or Co^{II}) ions, abbreviated as $[(\text{LS-Fe}^{\text{III}})_8(\text{Ni(or HS-Co}^{\text{II}}))_6]$. The core structure of **2**⁴⁺ can be recognized as a twelve-membered crown with an alternating arrangement of six Fe^{III} and six Co^{II} ions, cyanide bridged to form a ring motif, with two additional terminal Fe^{III} ions that are linked to the crown-like

[a] K. Mitsumoto, E. Oshiro, Prof. Dr. H. Nishikawa, Dr. T. Shiga, Dr. Y. Yamamura, Prof. Dr. K. Saito, Prof. Dr. H. Oshio
Graduate School of Pure and Applied Sciences
University of Tsukuba, Tennodai 1-1-1, Tsukuba 305-8571 (Japan)
Fax: (+81) 29-853-4238
E-mail: oshio@chem.tsukuba.ac.jp

Supporting information for this article is available on the WWW under <http://dx.doi.org/10.1002/chem.201101404>.

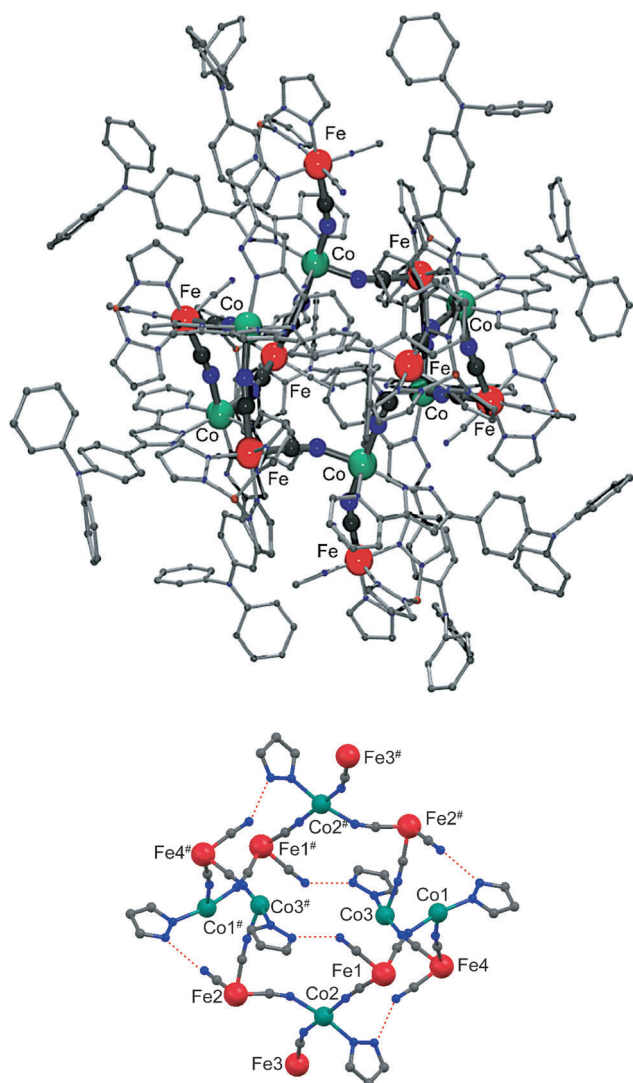


Figure 1. Structures of the cation 2^{4+} at 93 K and its cyanide bridged core. Dotted red lines represent the hydrogen bonds which support the core. Symmetry operation key: # = $1-x, y, z$.

core by cyanide bridges. The six coordination sites of each Fe^{III} ions in the crown are occupied by three nitrogen atoms from the tridentate tp^- ligand and the remaining facial positions are filled by the three cyanide carbon atoms. The terminal Fe^{III} ions are coordinated by three nitrogen atoms from the tp^- ligand and three cyanide ions—one of these cyanide ions bridges to a Co^{II} center and the remaining two act as monodentate ligands. The octahedral coordination environments of the Co1 and Co3 ions consist of N_6 donor sets from two bidentate ligands (HL) and two cyanide nitrogen atoms. The Co2 atom also has an octahedral coordination environment, but is connected to three cyanide nitrogen atoms, one HL ligand, and one CH_3CN molecule. The coordination bond lengths of the Ni^{II} and Co^{II} ions in **1** and **2** at 93 K are in the range of 2.072(8)–2.082(8) and 2.116(5)–2.122(5) Å, respectively, characteristic of divalent metal ions in the high-spin state. The Fe–C bond lengths are in the range of 1.872(12)–1.947(11) and 1.873(4)–1.949(7) Å for **1**

and **2**, respectively. In both complexes, six intramolecular hydrogen bonds are found between the uncoordinated cyanide nitrogen atoms and six protons of the pyrazole nitrogen atoms, supporting the large structures with a diameter of about 3 nm.

Magnetic properties: The dc magnetic susceptibility data of **1** were collected in the temperature range of 1.8–300 K, and the $\chi_m T$ versus T plot is shown in Figure 2. The $\chi_m T$ value at 300 K is $11.12 \text{ emu mol}^{-1} \text{ K}$, which is close to the value ($12.08 \text{ emu mol}^{-1} \text{ K}$) expected for eight uncorrelated $\text{LS-Fe}^{\text{III}}$ ($S=1/2$, $g_{\text{Fe}}=2.7$) and six Ni^{II} ions ($S=1$ and $g_{\text{Ni}}=2.1$). Relatively large g_{Fe} values have been previously reported for cyanide-bridged $\text{LS-Fe}^{\text{III}}$ complexes.^[2c,d,6] The $\chi_m T$ values gradually increased as the temperature was lowered and reached the maximum value of $46.18 \text{ emu mol}^{-1} \text{ K}$ at 1.8 K.

This suggests the occurrence of ferromagnetic interactions between the $\text{LS-Fe}^{\text{III}}$ and Ni^{II} ions, for which Curie and Weiss constants of $C=10.54 \text{ emu mol}^{-1} \text{ K}$ and $\theta=+10.73 \text{ K}$ were obtained. The magnetic data were analyzed by MAGPACK^[7] and fitted with a spin Hamiltonian of $H=-2J \cdot [S_{\text{Ni1}} \cdot (S_{\text{Fe1}}+S_{\text{Fe4}}) + S_{\text{Ni1}} \cdot (S_{\text{Fe1}}+S_{\text{Fe4}}) + S_{\text{Ni2}} \cdot (S_{\text{Fe1}}+S_{\text{Fe2}}+S_{\text{Fe3}}) + S_{\text{Ni2}} \cdot (S_{\text{Fe1}}+S_{\text{Fe2}}+S_{\text{Fe3}}) + S_{\text{Ni3}} \cdot (S_{\text{Fe2}}+S_{\text{Fe4}}) + S_{\text{Ni3}} \cdot (S_{\text{Fe2}}+S_{\text{Fe4}})]$, supposing the same isotropic exchange coupling constant (J) between the Fe^{III} and Ni^{II} pairs. The solid curve in Figure 2 was drawn using parameters of $J=+9.0 \text{ K}$ and $g=2.2$. The occurrence of ferromagnetic interactions can be understood by the orthogonal magnetic orbitals of the $\text{LS-Fe}^{\text{III}}$ ($d\pi$ spin) and Ni^{II} ($d\sigma$ spin) ions. The ac magnetic susceptibility measurements for **1** were performed in a 3 Oe ac field (Figure 2, inset). Both in- and out-of-phase signals showed frequency-dependence, suggesting that **1** is an SMM. At fixed temperatures from 1.80 to 2.05 K, Cole–Cole plots exhibited semicircles, which could be fitted to the extended Debye model,^[8] yielding α values of 0.09–0.18. The α parameter is the width of the distribution of the magnetic relaxation processes, and such small values correspond to a single relaxation process for **1** (Figure 3).

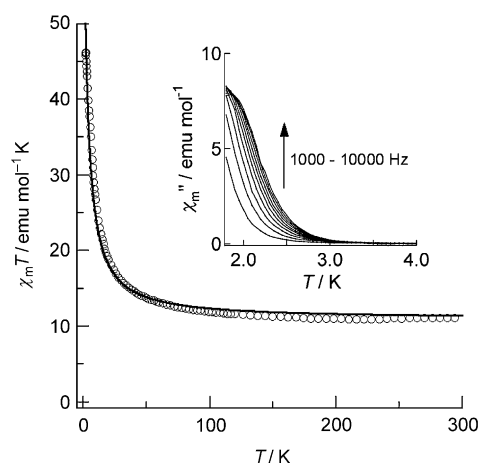


Figure 2. $\chi_m T$ versus T plot of **1** measured in an applied magnetic field of 500 Oe. The inset displays plots of out-of-phase AC susceptibility signals vs. temperature for **1**. The solid line was calculated by the parameters given in the text.

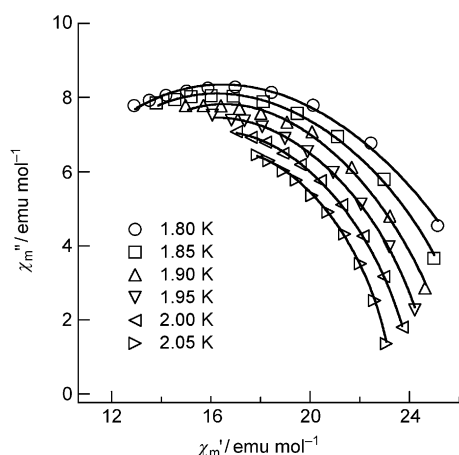


Figure 3. Cole–Cole diagrams of **1**. The solid lines represent least-square fits of the data to the Debye model.

Magnetic susceptibility measurements of **2** showed temperature profiles dependent upon the sample treatment (Figure 4). All measurements began at 1.8 K and the temperatures were increased. The fresh sample (open circle) showed rapidly increasing $\chi_m T$ values from 1.8 to 11.6 K, followed by a gradual increase to the $\chi_m T$ value of 21.34 emu mol^{−1} K at 300 K; the value at 300 K is close to the Curie constant (20.34 emu mol^{−1} K) obtained by summing the uncorrelated spins of eight LS-Fe^{III} ($S=1/2$) and six Co^{II} ions ($S=3/2$) with the $g_{\text{Fe}}=2.7$ and $g_{\text{Co}}=2.3$,^[2d,3b] corresponding with the cluster in the [(LS-Fe^{III})₈(HS-Co^{II})₆] state. The magnetic susceptibility data suggested that antiferromagnetic interactions between the Fe^{III} and Co^{II} ions were operative and the notable change of the $\chi_m T$ values in the low and intermediate temperature ranges might be due to the orbital contribution from the metal ions.

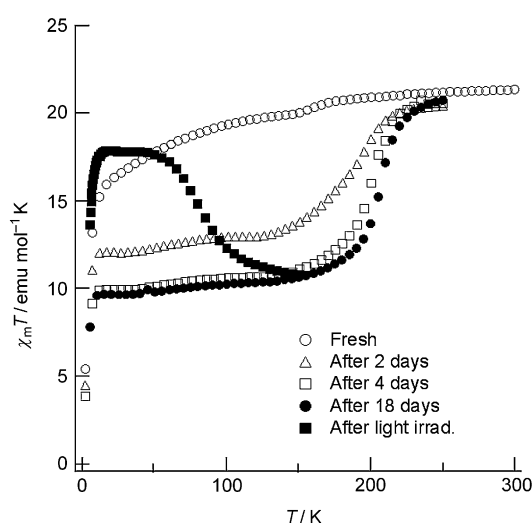


Figure 4. $\chi_m T$ versus T plots for **2** collected as a function of storage and light irradiation at 808 nm.

Storage of sample **2** at ambient temperature resulted in drastic changes in its magnetic behavior up to 18 days after which time no further change was observed (Figure 4). After 18 days of storage **2** was formulated as $[\text{Fe}_8\text{Co}_6(\text{CN})_{24}(\text{tp})_8(\text{HL})_{10}(\text{CH}_3\text{CN})_2][\text{PF}_6]_4 \cdot 5\text{H}_2\text{O}$ (Figure 4, filled circles; henceforth termed desolvated **2**) from elemental analysis and TGA data, and showed an almost constant $\chi_m T$ value (9.4–9.8 emu mol^{−1} K) in the temperature range of 20–180 K. A sigmoidal increase in $\chi_m T$ value began at 170 K, reaching $\chi_m T=20.0$ emu mol^{−1} K at 250 K. The $\chi_m T$ value of 9.4 emu mol^{−1} K at 20 K corresponds to the value (10.86 emu mol^{−1} K) expected for the [(LS-Fe^{II})₃(LS-Fe^{III})₅-(HS-Co^{II})₃(LS-Co^{III})₃] species, confirmed by Mössbauer spectroscopic measurements, and the value at 250 K is the same as that for the fresh sample **2**. It is, therefore, assumed that three electrons were transferred from the [(LS-Fe^{II})₃-(LS-Fe^{III})₅(HS-Co^{II})₃(LS-Co^{III})₃] to the [(LS-Fe^{III})₈(HS-Co^{II})₆] states upon the temperature increase. Note that no hysteresis was observed for desolvated **2**. When the sample was dried under vacuum for four days, only gradual increase of $\chi_m T$ values was observed from 13.7 emu mol^{−1} K at 10 K to 17.7 emu mol^{−1} K at 250 K, suggesting the absence of the electron transfer (see Figure S3 in the Supporting Information). Differential scanning calorimetry (DSC) measurements of desolvated **2** were performed (Figure S4 in the Supporting Information) and no peak was observed, indicating that negligibly small cooperativity exists in this transition. This agreed with the absence of hysteresis in the magnetic susceptibility data.

Thermogravimetric analysis (Figure S5 in the Supporting Information), elemental analysis, and ⁵⁷Fe Mössbauer spectral measurements were conducted to study the effect of storage and thermal treatment on **2**. The TGA of **2** displays a weight loss of 7.5 % upon heating from 40 to 73 °C, which correspond to the release of 14 acetonitrile molecules (calcd. 6.9 %). It is suggested that desolvated **2** has the formula $[\text{Fe}_8\text{Co}_6(\text{CN})_{24}(\text{tp})_8(\text{HL})_{10}(\text{CH}_3\text{CN})_2][\text{PF}_6]_4 \cdot 5\text{H}_2\text{O}$. The single crystal of desolvated **2** could not be obtained, and the powder XRD measurement for desolvated **2** was, therefore, performed and the result was depicted in Figure 5. The

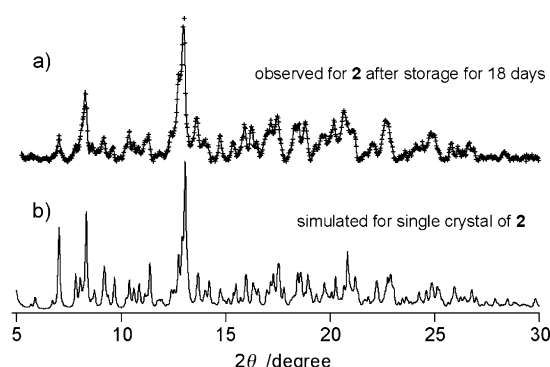


Figure 5. a) Powder XRD pattern of desolvated **2**. The solid line represent least-square fits of the data by using the parameters; $a=22.186(8)$, $b=26.406(5)$, $c=35.91(1)$ Å, $\beta=93.35(2)^\circ$. $R_p=0.090$, $R_{wp}=0.235$. b) The diffraction data generated using single-crystal structure analyses data.

Le Bail method^[9] was applied to estimate the lattice constants for the desolvated **2**, and the least-square calculation yielded similar lattice constants of $a=22.186(8)$, $b=26.406(5)$, $c=35.91(1)$ Å, $\beta=93.35(2)^\circ$, close to those for the fresh sample of **2**, with the same monoclinic space group, and R_p and R_{wp} residuals were 0.090 and 0.235, respectively. The result suggests that desolvated **2** retained a crystal structure similar to **2**.

Variable-temperature ^{57}Fe Mössbauer spectra: ^{57}Fe Mössbauer spectra of **1**, and fresh and desolvated **2** were measured at several temperatures (Figures S1 and S2 in the Supporting Information and Figure 6). The Mössbauer spectra of **1** at 20 K, and the fresh sample of **2** at 20 and 298 K all showed a single doublet, which were fitted with Mössbauer parameters (relative to iron steel) of $\delta=0.05$ and $\Delta E_Q=1.20\text{ mm s}^{-1}$, $\delta=-0.05$ and $\Delta E_Q=0.93\text{ mm s}^{-1}$, and $\delta=0.02$ and $\Delta E_Q=1.06\text{ mm s}^{-1}$, respectively, characteristic of LS- Fe^{III} species. Desolvated **2** showed a substantially different temperature profile from the fresh sample. The Mössbauer spectrum of desolvated **2** at 298 K is composed of one quadrupole doublet with $\delta=-0.03$ and $\Delta E_Q=0.96\text{ mm s}^{-1}$, characteristic of LS- Fe^{III} species. When the temperature was lowered, a new quadrupole doublet ($\delta=0.12$ and $\Delta E_Q=0.56\text{ mm s}^{-1}$) appeared at 250 K and its fraction increased as the temperature was lowered. The Mössbauer spectrum at 20 K showed two doublets with parameters of $\delta=0.06$ and $\Delta E_Q=1.24\text{ mm s}^{-1}$, and $\delta=0.18$ and $\Delta E_Q=0.58\text{ mm s}^{-1}$, characteristic of LS- Fe^{III} and LS- Fe^{II} species, respectively. Considering the peak area ratio of the two doublets ($\text{Fe}^{\text{III}}:\text{Fe}^{\text{II}}=$

0.64/0.36) and magnetic susceptibility data, three of the eight LS- Fe^{III} ions in the high-temperature (HT) phase ($[(\text{LS-Fe}^{\text{III}})_8(\text{HS-Co}^{\text{II}})_6]$) have changed to LS- Fe^{II} species in the low-temperature (LT) phase ($[(\text{LS-Fe}^{\text{II}})_3(\text{LS-Fe}^{\text{III}})_5(\text{HS-Co}^{\text{II}})_3(\text{LS-Co}^{\text{III}})_3]$); that is, three electrons were transferred from the Fe^{II} to Co^{III} sites followed by spin transition to the HS state on the Co^{II} sites. Note that no hysteresis was observed in the temperature dependence of the Mössbauer spectra. Thermodynamic parameters accompanying the transition were estimated by the temperature dependence of the LS- Fe^{III} fractions, assuming identical recoil free fractions of LS- Fe^{III} and LS- Fe^{II} species. The results gave enthalpy and entropy changes for the three-electron transfer process of $\Delta H=17.5\text{ kJ mol}^{-1}$ and $\Delta S=85.2\text{ J K}^{-1}\text{ mol}^{-1}$ with $T_c=205\text{ K}$ (Figure S6 in the Supporting Information).

The ETCST behavior was strongly dependent upon the release of the solvent molecules in **2**. The desolvation involves changes in hydrogen-bond networks between solvent molecules and terminal cyanide nitrogen atoms. Subtle changes in hydrogen bonds can lead to structure deformation and in some cases shifted redox potentials of metal centers, which may activate phase-transition-like ETCST. Such solvent effects have been also observed in $[\text{Co}(\text{tmphen})_2][\text{Fe}(\text{CN})_6]_2 \cdot 24\text{H}_2\text{O}$ (tmphen = 3,4,7,8-tetramethyl-1,10-phenanthroline)^[4b] and $[\text{Fe}(\text{tp})(\text{CN})_3]_2\text{Co}(\text{bpe}) \cdot 5\text{H}_2\text{O}$ (bpe = 1,2-bis(4-pyridyl)ethane).^[10]

Photomagnetic experiments: Light irradiation experiments using laser lights (405, 532, and 808 nm) were conducted on the desolvated **2** at 5 K in the SQUID magnetometer (Figure 4). Rapid increases of the $\chi_m T$ values were observed upon light irradiation (405 and 808 nm), and plots of χ_m versus irradiation time are shown in Figure S7 in the Supporting Information. The $\chi_m T$ values saturated at 13.6 and 11.2 $\text{emu mol}^{-1}\text{K}$ after irradiation (808 and 405 nm) for 4 and 8 h, respectively. No effect was observed following the irradiation 532 nm. Note that the χ_m values also increased when the lasers were turned off, and this is due to the decreased temperature upon turning off the laser lights. After turning off the laser source, the photoinduced species showed gradual increase of the $\chi_m T$ values as the temperatures were raised, reaching a plateau value of 17.8 $\text{emu mol}^{-1}\text{K}$ at 30 K, followed by a gradual decrease to 10.8 $\text{emu mol}^{-1}\text{K}$ at 150 K. The experiment suggests that the photoin-

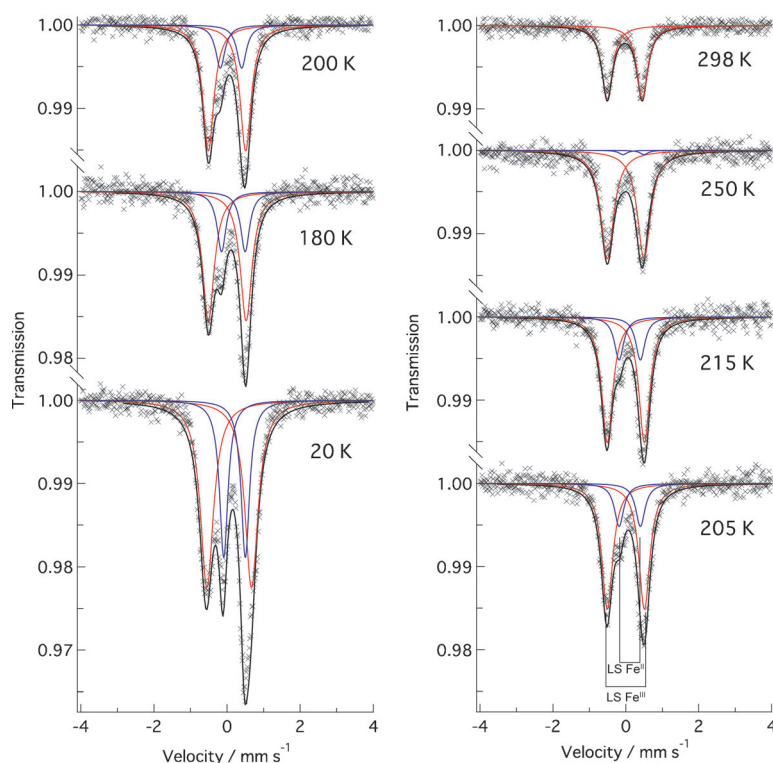


Figure 6. Temperature dependence of Mössbauer spectra of the desolvated **2**. The solid lines were calculated Lorentzian curves by using the parameters in the text.

duced transition of the LT phase, $[(\text{LS-Fe}^{\text{II}})_3(\text{LS-Fe}^{\text{III}})_5(\text{HS-Co}^{\text{II}})_3(\text{LS-Co}^{\text{III}})_3]$ to the metastable HT phase of $[(\text{LS-Fe}^{\text{II}})_8(\text{HS-Co}^{\text{II}})_6]$ occurred, which then thermally relaxed to the LT phase upon temperature increase. The light conversion ratio was 0.76, supposing $g_{\text{Fe}}=2.7$ and $g_{\text{Co}}=2.3$, respectively.^[2d,3b] Note that the photoinduced HT phase did not show out-of-phase signals in the ac susceptibility measurements, and that the reverse electron transfer in the metastable HT phase was not observed upon green light (532 nm) irradiation.

Conclusion

In summary, two novel tetradecanuclear complexes **1** and **2** were prepared. The capping ligand (HL) has an acidic proton and a bulky group, which stabilize a crown like core structure by intramolecular hydrogen bonds and by prohibiting polymerization reactions, respectively. Complex **1** is a single-molecule magnet, and **2**, after an 18 day storage period, showed thermal- and light-induced electron-transfer-coupled spin transition behavior.

Experimental Section

X-ray crystallography: A crystal was mounted on a glass capillary, and data were collected at -180°C (Bruker SMART APEXII diffractometer coupled with a CCD area detector with graphite monochromated $\text{MoK}\alpha$ ($\lambda=0.71073$ Å) radiation). The structure was solved using direct methods and expanded using Fourier techniques within the SHELXTL program.^[11] Empirical absorption corrections by SADABS (G.M. Sheldrick, 1994)^[12] were carried out. In the structure analyses, non-hydrogen atoms were refined with anisotropic thermal parameters. Hydrogen atoms were included in calculated positions and refined with isotropic thermal parameters riding on those of the parent atoms. PXRD data were collected with $\text{CuK}\alpha$ radiation on a MAC Science M18XHF-SRA, and an assessment of the crystal symmetry and of the lattice parameters was performed by the Le Bail Method.^[9]

Physical measurements: Magnetic susceptibility data were collected using a Quantum Design MPMS-5S SQUID magnetometer. Magnetization data for the fresh **1** and the desolvated **2** are shown in Figure S8 in the Supporting Information. The temperature scan rate was fixed to 1 K min^{-1} , and each measurement was performed 60 s after the temperature had stabilized. Magnetic data was corrected for the diamagnetic contribution associated with the sample holder, and the diamagnetism of the sample was corrected using Pascal's constants. Photomagnetic experiments were carried out using light from DPSS laser (405 nm; Edmund optics ZM18, 532 nm; Opto Tech KE.01, and 808 nm; Intelite I808–120G-CAP, 10 mW) and the light was guided by means of a flexible optical fiber (Newport F-MBD; 3 m length, 1.0 mm core size, 1.4 mm diameter) into the SQUID magnetometer. Irradiation was performed on the ground sample inside the SQUID sample chamber at 5 K. One end of the optical fiber was located 40 mm above the sample and the other was attached to the laser coupler (Body; Newport M-F-916T and lens; M-10X). The temperature dependence of magnetic susceptibility after light irradiation was measured using an applied magnetic field of 2 T and a scan rate of 1 K min^{-1} in scanning mode. Variable-temperature Mössbauer experiments were carried out using a $^{57}\text{Co/Rh}$ source in a constant-acceleration transmission spectrometer (Topologic Systems) equipped with an Iwatani HE05/CW404 Cryostat. The spectra were recorded in the temperature range of 20–298 K. The spectrometer was calibrated by using a standard $\alpha\text{-Fe}$ foil. Thermal analysis of desolvated **2** was carried

out in the temperature of 90–293 K, using a DSC (Perkin–Elmer Pyris 1). The mass of sample and temperature scan rate were 1.1465 mg and 2 K min^{-1} , respectively.

Materials: All solvents and chemicals were reagent-grade, purchased commercially, and used without further purification unless otherwise noted. Toluene was distilled from CaH_2 . 4'-(Diphenylamino)acetophenone was prepared by the literature method.^[13]

Synthesis of 3-[4-(diphenylamino)phenyl]-1-(2-pyridyl)propan-1,3-dione (HL): A solution of sodium ethoxide (641 mg, 9.47 mmol), 4'-(diphenylamino)acetophenone (1.50 g, 5.22 mmol) and ethyl 2-pyridinecarboxylate (1.72 g, 11.3 mmol) in toluene (150 mL) was refluxed under nitrogen for 1.5 h. The solvent was removed under reduce pressure, and the residue was acidified with aqueous acetic acid. The red precipitate was extracted with diethyl ether and dried with sodium sulfate. The solvent was evaporated and the crude product recrystallized from methanol to afford 1.84 g (4.73 mmol) of HL' as a red crystalline solid. Yield 91%; elemental analysis calcd (%) for $\text{C}_{26}\text{H}_{20}\text{N}_2\text{O}_2$: C 79.57, H 5.14, N 7.14; found: C 79.30, H 5.40, N 7.01; $^1\text{H NMR}$ (270 MHz, CDCl_3): $\delta=7.03$ (m, 2H), 7.28 (m, 6H), 7.32 (m, 4H), 7.43 (m, 1H), 7.46 (s, 1H), 7.85 (s, 1H), 7.93 (m, 2H), 8.11 (m, 1H), 8.68 ppm (m, 1H).

Synthesis of 3-(2-pyridyl)-5-[4-(diphenylamino)phenyl]-1H-pyrazole (HL): Hydrazine monohydrate (130 μL , 2.83 mmol) in methanol (10 mL) was added to a solution of HL' (1.00 g, 2.55 mmol) in CHCl_3 (20 mL) and the mixture was refluxed for 2 h. The solvent was evaporated and crude product was washed with acetonitrile. A yellow solid was yielded and recrystallized from CHCl_3 to afford 0.901 g (2.32 mmol) of ligand HL as a pale yellow crystalline solid. Yield 90%; elemental analysis calcd (%) for $\text{C}_{26}\text{H}_{20}\text{N}_4\cdot 0.2\text{H}_2\text{O}$: C 79.64, H 5.24, N 14.29; found: C 79.64, H 5.43, N 14.48. $^1\text{H NMR}$ (270 MHz, CDCl_3): $\delta=7.03$ (s, 2H), 7.25 (m, 6H), 7.66 (m, 6H), 7.82 (m, 2H), 8.63 ppm (m, 1H).

Synthesis of $[\text{Fe}_8\text{Ni}_6(\text{CN})_{24}(\text{tp})_8(\text{HL})_{10}(\text{CH}_3\text{CN})_2][\text{PF}_6]_{11}\cdot 11\text{CH}_3\text{CN}\cdot 7\text{H}_2\text{O}$ (1): $\text{Ni}[\text{BF}_4]\cdot 6\text{H}_2\text{O}$ (5.4 mg, 0.016 mmol) and ligand HL (12.5 mg, 0.032 mmol) were combined in acetonitrile (2 mL). The solution was stirred for 5 min. The resulting orange solution was combined with a solution of $n\text{Bu}_4\text{NPF}_6$ (31 mg, 0.08 mmol) and $n\text{Bu}_4\text{N}[\text{Fe}(\text{CN})_5(\text{tp})]$ (9.4 mg, 0.016 mmol) in acetonitrile (2 mL). Slow evaporation gave red crystals of **1**. Yield: 6.8 mg (41%); elemental analysis calcd (%) for $\text{C}_{360}\text{H}_{286}\text{N}_{114}\text{B}_8\text{F}_{24}\text{Fe}_8\text{Ni}_6\text{P}_4\cdot 7\text{H}_2\text{O}$: C 55.43, H 3.88, N 20.47; found: C 55.24, H 3.93, N 20.41. Crystal data for **1**: $\text{C}_{382}\text{H}_{333}\text{N}_{125}\text{B}_8\text{F}_{24}\text{Fe}_8\text{Ni}_6\text{O}_7\text{P}_4$, $M_r=8252.16$, monoclinic, space group $P2_1/n$, $a=21.937(1)$, $b=26.108(1)$, $c=35.764(2)$ Å, $\beta=93.227(3)^\circ$, $V=20449.9(16)$ Å³, $Z=2$, $T=93\text{ K}$, $\rho_{\text{calcd}}=1.340\text{ Mg m}^{-3}$, 63644 reflections collected of which 34345 were unique ($R_{\text{int}}=0.0869$), $R1 [I>2\sigma(I)]=0.1003$, $wR2=0.2516$.

Synthesis of $[\text{Fe}_8\text{Co}_6(\text{CN})_{24}(\text{tp})_8(\text{HL})_{10}(\text{CH}_3\text{CN})_2][\text{PF}_6]_{11}\cdot 14\text{CH}_3\text{CN}\cdot 5\text{H}_2\text{O}$ (2): Complex **2** was obtained by the same synthetic approach as **1**, but by using $\text{Co}[\text{BF}_4]\cdot 6\text{H}_2\text{O}$ instead of $\text{Ni}[\text{BF}_4]\cdot 6\text{H}_2\text{O}$. Yield: 7.3 mg (44%); elemental analysis calcd (%) for $\text{C}_{360}\text{H}_{286}\text{N}_{114}\text{B}_8\text{Co}_6\text{F}_{24}\text{Fe}_8\text{P}_4\cdot 5\text{H}_2\text{O}$: C 55.68, H 3.84, N 20.56; found (dried at ambient condition for 18 days): C 55.40, H 4.01, N 20.52. Crystal data for **2**: $\text{C}_{388}\text{H}_{338}\text{N}_{128}\text{B}_8\text{Co}_6\text{F}_{24}\text{Fe}_8\text{O}_5\text{P}_4$, $M_r=8340.60$, monoclinic, space group $P2_1/n$, $a=21.986(4)$, $b=26.275(4)$, $c=35.993(6)$ Å, $\beta=93.302(3)^\circ$, $V=20724(6)$ Å³, $Z=2$, $T=93\text{ K}$, $\rho_{\text{calcd}}=1.337\text{ Mg m}^{-3}$, 98297 reflections collected of which 36413 were unique ($R_{\text{int}}=0.0804$), $R1 [I>2\sigma(I)]=0.0790$, $wR2=0.2155$.

CCDC-802155 (**1**) and 802156 (**2**) contain the supplementary crystallographic data for this paper. These data can be obtained free of charge from The Cambridge Crystallographic Data Centre via www.ccdc.cam.ac.uk/data_request/cif.

Acknowledgements

This work was supported by a Grant in Aid for Scientific Research for Priority Area “Coordination Programming” (area 2107) from MEXT (Japan) and by the JSPS.

- [1] a) A. N. Holden, B. T. Matthias, P. W. Anderson, H. W. Lewis, *Phys. Rev.* **1956**, *102*, 1463–1463; b) S. Ferlay, T. Mallah, R. Ouahès, P. Veillet, M. Verdaguer, *Nature* **1995**, *378*, 701–703; c) P. Franz, C. Ambrus, A. Hauser, D. Chernyshov, M. Hostettler, J. Hauser, L. Keller, K. Krämer, H. Stoeckli-Evans, P. Pattison, H.-B. Bürgi, S. Decurtins, *J. Am. Chem. Soc.* **2004**, *126*, 16472–16477; d) O. Sato, T. Iyoda, A. Fujishima, K. Hashimoto, *Science* **1996**, *271*, 49–51; e) O. Sato, T. Iyoda, A. Fujishima, K. Hashimoto, *Science* **1996**, *272*, 704–705; f) S. Ohkoshi, H. Tokoro, T. Matsuda, H. Takahashi, H. Irie, K. Hashimoto, *Angew. Chem.* **2007**, *119*, 3302–3305; *Angew. Chem. Int. Ed.* **2007**, *46*, 3238–3241; g) S. Ohkoshi, K. Nakagawa, K. Tomono, K. Imoto, Y. Tsunobuchi, H. Tokoro, *J. Am. Chem. Soc.* **2010**, *132*, 6620–6621; h) Y. Moritomo, F. Nakada, H. Kamioka, T. Hozumi, S. Ohkoshi, *Phys. Rev. B* **2007**, *75*, 214110.
- [2] a) H. Oshio, H. Onodera, T. Ito, *Chem. Eur. J.* **2003**, *9*, 3946–3950; b) M. Nihei, M. Ui, M. Yokota, L. Han, A. Maeda, H. Kishida, H. Okamoto, H. Oshio, *Angew. Chem.* **2005**, *117*, 6642–6645; *Angew. Chem. Int. Ed.* **2005**, *44*, 6484–6487; c) D. Li, S. Parkin, G. Wang, G. T. Yee, S. M. Holmes, *Inorg. Chem.* **2006**, *45*, 1951–1959; d) Y. Zhang, D. Li, R. Clérac, M. Kalisz, C. Mathonière, S. M. Holmes, *Angew. Chem.* **2010**, *122*, 3840–3844; *Angew. Chem. Int. Ed.* **2010**, *49*, 3752–3759; e) J. Kim, S. Han, I. K. Cho, K. Y. Choi, M. Heu, S. Yoon, B. J. Suh, *Polyhedron* **2004**, *23*, 1333–1339; f) M. Nihei, Y. Sekine, N. Suganami, H. Oshio, *Chem. Lett.* **2010**, *39*, 978–979.
- [3] a) D. Li, S. Parkin, G. Wang, G. T. Yee, R. Clérac, W. Wernsdorfer, S. M. Holmes, *J. Am. Chem. Soc.* **2006**, *128*, 4214–4215; b) D. Li, R. Clérac, O. Roubeau, E. Harté, C. Mathonière, R. L. Bris, S. M. Holmes, *J. Am. Chem. Soc.* **2008**, *130*, 252–258; c) M. Nihei, M. Ui, N. Hoshino, H. Oshio, *Inorg. Chem.* **2008**, *47*, 6106–6108.
- [4] a) C. P. Berlinguette, D. Vaughn, C. Cañada-Vilalta, J. R. Galán-Mascarós, K. R. Dunbar, *Angew. Chem.* **2003**, *115*, 1561–1564; *Angew. Chem. Int. Ed.* **2003**, *42*, 1523–1526; b) C. P. Berlinguette, A. Dragulescu-Andrasi, A. Sieber, H. U. Güdel, C. Achim, K. R. Dunbar, *J. Am. Chem. Soc.* **2005**, *127*, 6766–6779; c) M. G. Hilfiger, M. Chen, T. V. Brinzari, T. M. Nocera, M. Shatruk, D. T. Petasis, J. L. Musfeldt, C. Achim, K. R. Dunbar, *Angew. Chem.* **2010**, *122*, 1452–1455; *Angew. Chem. Int. Ed.* **2010**, *49*, 1410–1413.
- [5] a) W. Liu, K. Lee, M. Park, R. P. John, D. Moon, Y. Zou, X. Liu, H. C. Ri, G. H. Kim, M. S. Lah, *Inorg. Chem.* **2008**, *47*, 8807–8812; b) K. Nakabayashi, Y. Ozaki, M. Kawano, M. Fujita, *Angew. Chem.* **2008**, *120*, 2076–2078; *Angew. Chem. Int. Ed.* **2008**, *47*, 2046–2048; c) A. M. Todea, A. Merca, H. Bögge, J. Slagereen, M. Dressel, L. Engelhardt, M. Luban, T. Glaser, M. Henry, A. Müller, *Angew. Chem.* **2007**, *119*, 6218–6222; *Angew. Chem. Int. Ed.* **2007**, *46*, 6106–6110; d) D. Furusho, K. Nishi, T. Hashibe, T. Fujinami, H. Hagiwara, N. Matsumoto, M. A. Halcrow, S. Iijima, Y. Sunatsuki, M. Kojima, *Chem. Lett.* **2011**, *40*, 72–74.
- [6] D. Li, R. Clérac, G. Wang, G. T. Yee, S. M. Holmes, *Eur. J. Inorg. Chem.* **2007**, 1341–1346.
- [7] J. J. Borrás-Almenar, J. M. Clemente-Juan, E. Coronado, B. S. Tsukerblat, *J. Comput. Chem.* **2001**, *22*, 985–991.
- [8] a) M. H. Zeng, M. X. Yao, H. Liang, W. X. Zhang, X. M. Chen, *Angew. Chem.* **2007**, *119*, 1864–1867; *Angew. Chem. Int. Ed.* **2007**, *46*, 1832–1835; b) N. Lopez, A. V. Prosvirin, H. Zhao, W. Wernsdorfer, K. R. Dunbar, *Chem. Eur. J.* **2009**, *15*, 11390–11400; c) Z.-M. Sun, A. V. Prosvirin, H. H. Zhao, J. G. Mao, K. R. Dunbar, *J. Appl. Phys.* **2005**, *97*, 10B305; d) G. Q. Bian, T. Kuroda-Sowa, T. Nogami, K. Sugimoto, M. Maekawa, M. Munakata, H. Miyasaka, M. Yamashita, *Bull. Chem. Soc. Jpn.* **2005**, *78*, 1032–1039; e) M. Haryono, M. Kalisz, R. Sibille, R. Lescouëzec, C. Fave, G. T. Allard, Y. Li, M. Seuleiman, H. Rousselière, A. M. Balkhy, J. C. Lacroix, Y. Journaux, *Dalton Trans.* **2010**, *39*, 4751–4756.
- [9] A. Le Bail, H. Duroy, J. L. Fourquet, *Mater. Res. Bull.* **1988**, *23*, 447–452.
- [10] T. Liu, Y.-J. Zhang, S. Kanegawa, O. Sato, *Angew. Chem.* **2010**, *122*, 8827–8830; *Angew. Chem. Int. Ed.* **2010**, *49*, 8645–8648.
- [11] G. M. Sheldrick, SADABS, Bruker AXS, Madison, USA, **1997**.
- [12] G. M. Sheldrick, SHELXS97 and SHELXL97, University of Göttingen, Germany, **1997**.
- [13] H. L. Wang, B. Zhang, W. Y. Xu, Y. Q. Bai, H. Wu, *Acta Crystallogr. Sect. E* **2007**, *63*, o2648–o2649.

Received: May 9, 2011
Published online: August 9, 2011